A CFD INVESTIGATION ON THE EFFECTS OF

ENTRANCE CROSSFLOW DIRECTIONS TO FILM-COOLING HOLES

A. Kohli and K. A. Thole
Mechanical Engineering Department
University of Wiscsonsin
Madison, Wisconsin 53706

ABSTRACT

Further increases in film-cooling effectiveness is a primary goal of the gas turbine industry. One effect that has been, for the most part, ignored in film-cooling studies, is the effect that a cross-flow at the hole entrance (which would occur on the internal side of the turbine blade) has on exiting jet and the cooling capabilities of that jet. This CFD study has investigated how different coolant flow directions at the inlet to either a round cooling hole or a shaped cooling hole can affect the overall cooling performance of that jet. The shaped cooling hole, which is fully expanded at 15°, had a lateral hole spacing of six hole diameters while the round hole had a lateral hole spacing of three hole diameters. Engine conditions were simulated in that a density ratio of two was used with a blowing ratio of $M = 0.5$ for the round hole and $M = 1$ for the shaped cooling hole. This allowed a direct comparison between the two geometries on the basis of equal coolant per blade pitch. The coolant supply flows at the hole entrance were considered to be either a plenum condition; parallel and in the same or opposite direction of the mainstream at the hole exit; or perpendicular to the mainstream at the hole exit. All of the flowing supplies had a channel Reynolds number of 30,000 and a channel height of 3 diameters. Results indicate that for the round cooling hole the adiabatic effectiveness values for a plenum and supply channel flow at 90° were essentially the same even though the flow features inside the coolant hole were significantly different. The adiabatic effectiveness for the shaped cooling hole, however, was significantly reduced when the coolant supply flow was perpendicular to the mainstream flow direction.

INTRODUCTION

The high performance gas turbines of today are pushing the inlet temperature to higher levels in order to improve their thermal efficiency. The practical limit for the inlet temperature is set by the material composition and convective cooling strategies for the blades. Film-cooling is a process whereby compressor bleed air, which bypasses the combustor, is injected through discrete holes in the blade surface. This cooling method has been and is currently continuing to be refined to further aid in prolonging the blade life.

One effect that has been, for the most part, ignored in evaluating the film-cooling process is the effect that the crossflow present at the hole entrance has on the cooling characteristics. For the remainder of this paper the crossflow at the exit to the film-cooling hole will be referred to as the mainstream and the crossflow at the entrance to the film-cooling hole will be referred to as the coolant supply. As film cooling holes on the turbine blade are typically short ($3 \le L/D \le 6$), the flow coming out of these holes is not fully developed. Most experimental and CFD studies on film cooling have been performed using a stagnant plenum supplying the film-cooling holes. Although a stagnant plenum may be applicable in the leading edge of a turbine blade, for example, the coolant supply in the main body of the blade can be completely different. Alternatively, the coolant can be supplied to the cooling hole from a supply channel having a Reynolds number which can range between $7000 < Re_H < 90{,}000$ as reported by Han (1984). Furthermore, in the process of routing the air through the blade to enhance internal side convection, the flow in the supply channel could potentially be in various directions with respect to the film cooling hole entrance.

This CFD study investigates the effect of the coolant supply channel on the characteristics of the cooling film. The supply channel crossflow at the hole entrance was considered to be co-flowing ($\phi = 0°$), perpendicular ($\phi = 90°$), or counter-flowing ($\phi = 180°$) with respect to the mainstream. These results are compared to the case in which the coolant is supplied to the hole by a stagnant plenum, that which has been commonly modeled both experimentally and numerically in past studies. Two typical film cooling hole geometries are investigated with both having an $L/D = 4$ and inclination angle of $\alpha = 35°$. The two hole geometries include a round hole and a shaped hole that has a fully expanded exit. All calculations are performed for a fixed density ratio of $DR = 2$. also typical of actual turbine conditions. The following sections discuss past relevant studies, the CFD method used in this study, the predictions for the round and shaped cooling hole, and finally give some conclusions.

PAST STUDIES

Since 1970, there has been an abundance of film-cooling studies presented in the literature. This published film-cooling data, however, is predominantly surface measurements representing adiabatic effectivenesses (using either heat transfer or mass transfer measurements). One of the more relevant studies to the work presented here was work reported by Goldstein, Eckert, and Burggraf (1974). Goldstein, et al. showed that when they laterally expanded the cooling hole by 10°, improved adiabatic effectiveness values were measured for a blowing ratio as high as $M = 2.2$. In contrast, a round hole showed that the jet detached from the surface causing low adiabatic effectiveness levels at much lower blowing ratios.

Among the first in-depth flowfield results for relevant film-cooling geometries were reported by Pietrzyk, et al. (1989). Pietrzyk, et al. (1989) measured flows from inclined jets exiting from a row of round film cooling holes with a length-to-diameter ratio of $L/D = 3.5$. This study hypothesized a separation region occurring at the inlet to the cooling hole based on the high turbulence levels and skewed jet velocity profile that they measured exiting the cooling hole. This separation region was also predicted by a CFD study done by Leylek and Zerkle (1994).

In a study involving round film-cooling holes with an $L/D = 4$, Schmidt, et al. (1996) showed that compared to the data from Sinha, et al. (1991), who used an $L/D = 1.75$, a clear detachment and reattachment of the jet from the downstream surface occurred for the shorter $L/D = 1.75$, but not for the longer $L/D = 4$ at a blowing ratio of $M = 1$ and a density ratio of $DR = 1.6$. The importance of the exiting jet profile on surface heat transfer is critical and best described by Garg and Gaugler's (1995) study. The numerical results predicted by Garg and Gaugler showed large differences in blade surface heat transfer depending upon the exiting jet velocity and temperature profiles for several film-cooled turbine blades. Garg and Gaugler presented heat transfer predictions that had differences by as much as 50-60% depending upon whether a parabolic or one-seventh jet profile was assumed to exit the cooling hole.

Although, the literature indicates that there is a large effect on the surface temperatures as a result of the exiting velocity profile, there have been only a few studies that have investigated the effect of the supply channel crossflow, which in fact can influence the exiting profiles. The studies that have considered the crossflow effect are discussed below.

Hay, et al. (1983) showed that the crossflow at the jet entrance had a large effect on the discharge coefficient relative to the effect of the crossflow at the hole exit. For example in the case where the crossflow at the hole entrance, which was parallel and in the same direction as the flow at the hole exit, increased from $Ma_c = 0$ to $Ma_c = 0.4$ the discharge coefficient increased by 30%. In contrast, as the exit Mach flow increased from $Ma_\infty = 0$ to $Ma_\infty = 0.5$, the discharge coefficient decreased by only 10% for pressure ratios of $1.05 < Pt,c / p_\infty < 1.4$ and remained constant when the pressure ratios were $Pt,c / p_\infty > 1.4$. Similar results were obtained in a recent study involving film-cooling holes with expanded exits by Gritsch, et al. (1997a). They reported an increase in the discharge coefficient of 40% when the crossflow at the hole entrance was increased from $Ma_c = 0$ to $Ma_c = 0.6$.

Berhe and Patankar (1996) performed a CFD study for round film cooling holes in which they investigated the effect of the plenum flow direction. Note that their studies, however, are significantly different than the study presented in this paper in that the results from this paper are for a condition where there is a through flow in the channel supplying the coolant hole whereas Berhe and Patankar used a plenum supplied from different directions. The results of Berhe and Patankar showed at a blowing ratio of $M = 0.5$ and a plenum height of $1D$, the adiabatic effectiveness was reduced significantly when the coolant was introduced into the plenum flowing in the parallel but opposite direction (counter-flowing) as the flow at the hole exit.

The experimental studies by Thole, et al. (1997), and Gritsch, et al. (1997b) have included flowfield and surface adiabatic effectiveness measurements for round and shaped cooling holes. The flowfield measurements, reported by Thole, et al. (1997), for a round cooling hole inclined at 30° with $L/D = 6$ showed a significant effect on the exiting velocity profile of the jet as well as where the peak turbulence level occurred. The results showed that for entrance crossflow Mach numbers of $Ma_c = 0$ (representing a plenum) and $Ma_c = 0.5$, a separation region occurred either on the leeward and windward side of the cooling hole entrances, respectively. As a result of this separation region, the cooling jet exited in a skewed manner with very high turbulence levels. For the case of an entrance crossflow Mach number of $Ma_c = 0.3$, which was close to the mainstream Mach number of $Ma_\infty = 0.25$, there was no evidence to support the fact that there was a large separation region.

The fully expanded (at 15°) cooling hole measurements, reported by Gritsch, et al. (1997a) showed that for blowing ratios of $M = 1$ and 1.5 reduced values of laterally averaged adiabatic effectivenesses occurred when the supply channel crossflow was turned perpendicular ($\phi = 90°$)

Nomenclature

D = diameter of film cooling hole
DR = density ratio, defined as $DR = \rho/\rho_\infty$
H = height of supply channel
k = turbulent kinetic energy, defined as $k = 3/2\ (U_\infty Tu(\%)/100)^2$
L = length of film cooling hole
L_M = cylindrical metering length for shaped hole
M = blowing ratio defined as $M = \rho_j V_j / \rho_\infty U_\infty$
Ma = Mach number
P = pitch distance between film cooling holes
Re_H = Reynolds number based on inlet velocity and channel height
Tu = turbulence level defined as $Tu = 100\ (2/3\ k)^{0.5} / U_\infty$
U = velocity component in the streamwise direction
V = velocity magnitude
VR = velocity ratio defined as $VR = V_j / U_\infty$
x = streamwise direction measured from hole exit centerline
y = vertical direction measured at hole exit centerline
z = spanwise direction measured from hole exit centerline

Greek

α = injection angle of film cooling holes
ε = turbulent dissipation rate, defined as $\varepsilon = C_\mu^{3/4} k^{3/2} / D$
ρ = density
ϕ = angle between supply channel flow and mainstream
η = adiabatic effectiveness, defined as $\eta = (T_{aw} - T_\infty) / (T_j - T_\infty)$
Θ = normalized temperature, defined as $\Theta = (T - T_\infty) / (T_j - T_\infty)$

Subscripts

aw = adiabatic wall
c = coolant
Cl = centerline
∞ = freestream
j = jet

Superscripts

$\bar{}$ = laterally averaged
$=$ = area averaged

as compared to the case when there was a co-flowing supply ($\phi = 0°$). For the same mainstream and coolant supply channel conditions, their results for the round hole indicated no effect at a near-optimal blowing ratio of $M = 0.5$. However, for the round hole the opposite trend to the shaped hole occurred at higher blowing ratios of $M = 1$ and 1.5 where higher values of laterally averaged effectiveness occurred for the $\phi = 90°$ supply flow direction as compared to the $\phi = 0°$ supply flow direction. Since the jet is known to separate at a blowing ratio of $M = 1$ for a round hole (Sinha, et al., 1991), this opposite trend may be occurring due to the swirling of the jet inside the hole, which will be discussed later in this paper, thereby causing a reduction in the severity of the jet detachment.

Results from these past studies have pointed to the importance of understanding the entrance crossflow effect to the cooling coverage that can be obtained by a film-cooling hole. The contribution, then, of this study is to evaluate the effect of different crossflow directions at the entrance to film-cooling holes, both round and shaped, at realistic engine conditions with a density ratio of $DR = 2$ and a supply channel Reynolds number of $Re_H = 30{,}000$. Both the adiabatic effectiveness as well as the flow fields will be discussed to give a good physical understanding of the entrance crossflow effects. This information is useful for two major reasons. First, a turbine blade designer can use this information in that he or she may consider changing the inner blade geometry such that better film-cooling coverage can be easily achieved. Second, a turbine durability engineer can use this information in that he or she may achieve better estimates for blade life.

HOLE GEOMETRIES AND TEST CASES

Two different hole geometries, one round and the other shaped, were considered in this study. Both holes were angled at $\alpha = 35°$ to the mainstream, had a hole diameter of $D = 12.7$ mm, and a length-to-diameter ratio of $L/D = 4$ as shown in Figure 1. The shaped hole had a cylindrical metering length of $L_M/D = 2$, after which it expanded at 15° in both the forward and lateral directions. The inside corners of the shaped cooling hole were rounded to have a radius of one-half the hole diameter. At the hole exit plane, the shaped hole had a streamwise extent of $3.8D$ and a spanwise extent of $1.8D$. A hole pitch of $P/D = 3$ was used for the round holes while the shaped holes were considered to be spaced $P/D = 6$ apart. The hole pitch determined the spanwise extent of the computational domain and location of the symmetry boundary conditions.

While the round cooling hole is typical of that appearing in the literature, the shaped cooling hole is similar to that reported by Wittig, et al. (1996), which was derived from several European gas turbine companies. Note that the coordinates for both of the cooling holes are measured at the exit plane of the hole and at the hole centerline. The blowing ratio for the round hole was chosen to represent near optimal conditions (Sinha, et al., 1991) at $M = 0.5$, whereas the blowing ratio for the shaped hole was chosen higher at $M = 1$ since that is more representative of engine operating conditions. Moreover, these two conditions, given the fact that the round hole has half the pitch spacing between holes compared to the shaped hole, represents the same given coolant mass flux per unit span. This means the results for the two hole shapes can be compared directly from a design point of view based on coolant usage.

Table 1 shows the four different crossflow cases considered for the coolant supply channel. These four cases were a plenum supply, a supply channel that was co-flowing ($\phi = 0°$) or counter-flowing ($\phi = 180°$), and a supply channel that was flowing in a direction perpendicular to the mainstream flow ($\phi = 90°$). For the $\phi = 0°$, 90°, and 180° cases, the supply channel velocity and height was set to 3.5 m/s and $H/D = 3$, which provided a channel Reynolds number of $Re_H = 30{,}000$. The mainstream velocity at the hole exit was 10 m/s except for the round hole plenum case where the mainstream velocity was set to 20 m/s which allowed comparisons to data given by Pietrzyk, et al. (1989). A typical engine density ratio (coolant-to-mainstream) of $DR = 2$ was considered for all of the cases.

Table 1. CFD Test matrix

Hole Geometry	Plenum	$\phi = 0°$	$\phi = 90°$	$\phi = 180°$
Round	$M = 0.5$		$M = 0.5$	
Shaped	$M = 1$	$M = 1$	$M = 1$	$M = 1$

COMPUTATIONAL DOMAIN

The computational domain consists of the mainstream flow, film-cooling hole, and the supply channel as indicated in Figure 2. The streamwise extent of the computational domain, similar to the past CFD studies of Leylek and Zerkle (1994) and Berhe and Patankar(1996), was $-19 \le x/D \le 30$. A boundary condition of a uniform inlet velocity is applied at the upstream end of the domain. This is consistent with Pietrzyk et al. (1989) who reported that a fresh turbulent boundary layer started at $x/D = -19$ on the test plate. For the present study, with a freestream velocity of $U_\infty = 10$ m/s, this resulted in a Reynolds number of $Re_\theta = 560$ upstream of the film-cooling holes. An outflow boundary condition is applied at the downstream end of the domain since gradients in the streamwise direction are expected to be small at $x/D = 30$. In the vertical direction, the computational domain extends out to $y/D = 10$ which is sufficiently far away from the film-cooling flowfield to allow a zero gradient boundary condition to be imposed. A zero heat flux boundary condition is imposed on all walls including the film-cooling hole.

For the case where the coolant supply channel is a plenum and for the cases when flow in the supply channel is co-flowing ($\phi = 0°$) or counter-flowing ($\phi = 180°$) to that of the mainstream flow, a symmetry

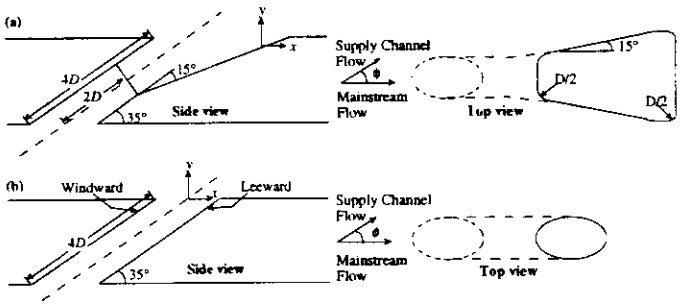

Fig. 1 Schematic of the (a) shaped and (b) round film cooling hole geometry.

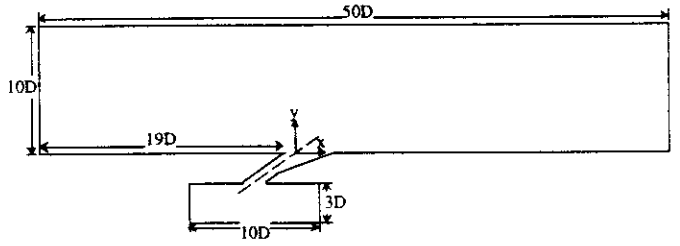

Fig. 2 Computational domain for both the shaped and round (not shown) holes. Note that the coordinate origin is located at the hole centerline with the +z direction coming out of the page.

condition is applied on both the jet centerline and the half-pitch line. Therefore, for these cases the spanwise extent of the computational domain is only $-3 < z/D < 0$ and flow in only half the film-cooling hole is modeled. When the flow in the supply channel is in a direction perpendicular ($\phi = 90°$) to that of the mainstream flow, this symmetry condition cannot be applied at the jet centerline. In this case, the entire film-cooling hole is modeled and the domain extends from $-3 < z/D < 3$ with periodic boundary conditions applied at both half-pitch lines.

The supply channel has a height of $H/D = 3$ and extends $5D$ upstream and $5D$ downstream of the entrance to the film-cooling hole. A uniform inlet velocity of 3.5 m/s is imposed at the upstream end of the supply channel while the velocity at the outlet of the supply channel was set according to the desired blowing ratio. Mass conservation was checked to insure that the correct blowing ratio was maintained through the cooling hole and was within 0.1% of the desired value. The boundary layer developed along the supply channel walls and was 4 mm thick ($0.3D$) at a location one diameter upstream of the hole entrance. For the supply channel flow in a direction normal to the mainstream flow, the supply channel was rotated about its vertical axis by 90° and flow was considered to be in the -z direction. For the plenum case, the same supply channel geometry was used with an appropriate inlet velocity imposed at the bottom face of the entire channel length.

SOLUTION METHODOLOGY

These CFD simulations were completed with a software package by Fluent, Inc., which included a pre-processor (Geomesh), an interior mesh generator (Tgrid), and a 3D Navier-Stokes solver (FLUENT/UNS). An unstructured mesh was used for these studies. The FLUENT/UNS solver has the ability to adapt solutions based on gradients of all flow variables in order to achieve grid independent results. The solution methodology used in this study is similar to that described by Walters and Leylek (1996). Second-order discretization was used for the governing equations for momentum, energy, and turbulence. Turbulence closure was achieved by using the standard k-ε model with nonequlibrium wall functions (Kim and Choudhury, 1995). As recommended in the FLUENT User's Guide (1996), the nonequlibrium wall functions were used since they are more appropriate compared to the standard wall functions for complex flows involving separation and reattachment, which is consistent for film-cooling flows. Note that default constants for the Launder and Spalding (1974) k-ε model were used without any adjustment for all the simulations in this study.

Figure 3 shows a cross-section on the hole centerline of the initial unstructured grid used for the shaped film-cooling calculations. The average cell skewness for the tetrahedral unstructured grids was 0.33 with the cells near the wall maintaining an average height of $y^+ = 20$, which was required in order to use the wall function approach correctly. The average number of cells for the round hole was 120,000 for the half-hole simulations and 180,000 for the entire hole. The average number of cells for the shaped hole simulations was 180,000 for the half-hole simulations and 220,000 cells for the entire hole. Typically, each simulation was split into six partitions and was run in parallel on an IBM SP/2 computer. Solution initialization was done using the freestream velocity and temperature and flow solutions were obtained using an under-relaxation parameter of 0.2 for momentum, k and ε. For each case, solution to the momentum equation (with the supply channel at the freestream temperature) was obtained before beginning the energy solution (with the supply channel temperature such that $DR = 2$).

To insure grid independence, the gradient adaption feature in FLUENT/UNS was used to refine the grid. Adaption was done based on the gradients of temperature and turbulent kinetic energy by using the hanging node method which generates a finer grid without increasing cell skewness. Typically, this adaption added about 40,000 cells to the initial grid, mainly concentrated near the film cooling hole. To insure that a grid independent solution was obtained, it was verified that further gradient adaption changed the value of laterally averaged effectiveness monitored near the hole by less than $\Delta\bar{\eta} = 0.005$.

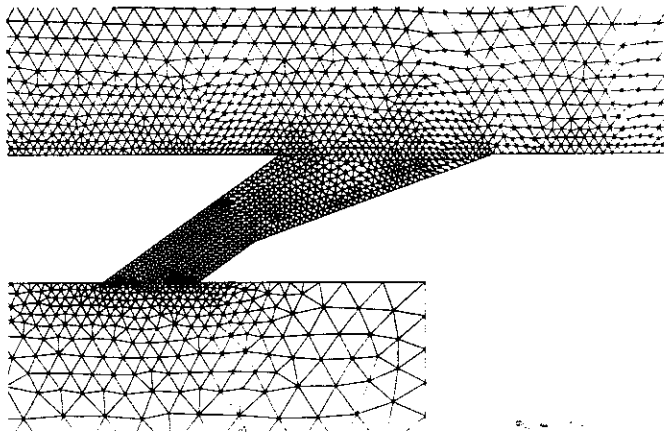

Fig. 3 Close-up view of the initial grid on the centerline plane for the shaped hole.

The convergence criteria for these computations involved two steps. First, convergence was considered to be close when the exiting mass flowrate was within 0.01% of that entering the computational domain, which typically required around 2500 iterations. This took about three days of run time on the IBM SP/2 and all residual levels were reduced by at least three orders of magnitude. The solution was then adapted as described above and run for 2000 iterations. For this final solution, values of centerline and laterally averaged effectiveness monitored near the hole over the last 1000 iterations changed by less than $\Delta\eta_{cl} = 0.001$ and $\Delta\bar{\eta} = 0.0001$ respectively. For the same number of iterations the velocity magnitude and turbulence level monitored near the film-cooling hole changed less than $\Delta V = 0.003$ m/s and $\Delta Tu = 0.007\%$ respectively.

RESULTS

The following sections discuss the predictions of the flow field, thermal field, and surface adiabatic effectiveness levels obtained for the test matrix given in Table 1. The results presented in this study focus on the flow features inside the coolant hole as they dictate the changes in adiabatic effectiveness resulting from changes in the flow direction of the supply channel. The round hole results are first described which are then followed by the shaped hole results.

Round Hole Results

The blowing and density ratios remained constant at $M = 0.5$ and $DR = 2$ for all of the round hole cases discussed in this section. For the round hole, only the plenum condition and the $\phi = 90°$ crossflow direction were computed. The velocity vectors on the jet centerline for both the plenum condition and $\phi = 90°$ crossflow are shown in Figure 4. For the plenum case, the vectors clearly show the formation of a separation region on the leeward side of the cooling hole caused by the large turning angle encountered by the jet fluid, as first identified by Pietrzyk, et al. (1989). This separation region causes the flow to accelerate on the windward side of the hole. The separation region can also be seen for $\phi = 90°$ although the jet centerline is no longer a plane of symmetry.

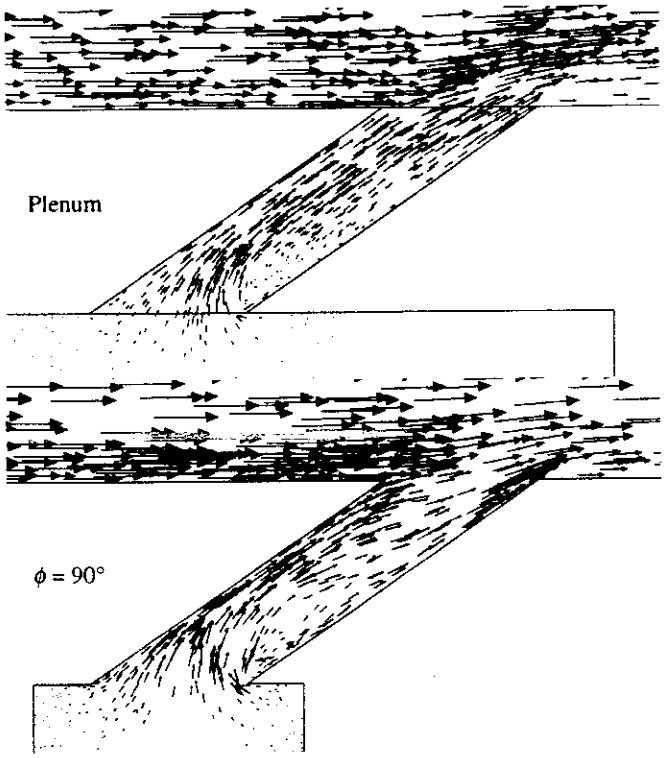

Fig. 4 Velocity vectors at the round hole centerline for the plenum condition and ϕ= 90°.

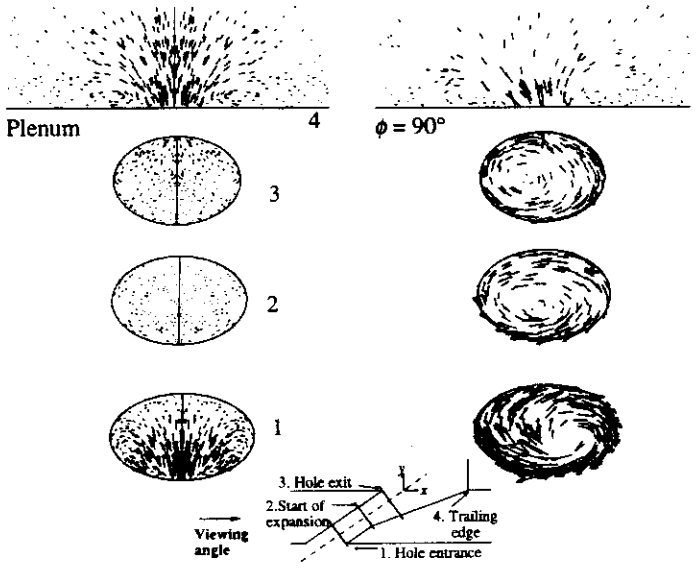

Fig. 5 Velocity vectors inside the round hole and at trailing edge of the hole exit for plenum condition and ϕ= 90°.

In-plane velocity vectors at three planes inside the round hole and at the trailing edge of the hole exit, are shown in Figure 5 (see schematic in Figure 5 for exact locations of the in-hole planes) for both the plenum condition and $\phi = 90°$. Vectors for the plenum condition show the formation of a counter-rotating vortex motion inside the film-cooling hole, caused by the flow turning over the separation bubble on the leeward

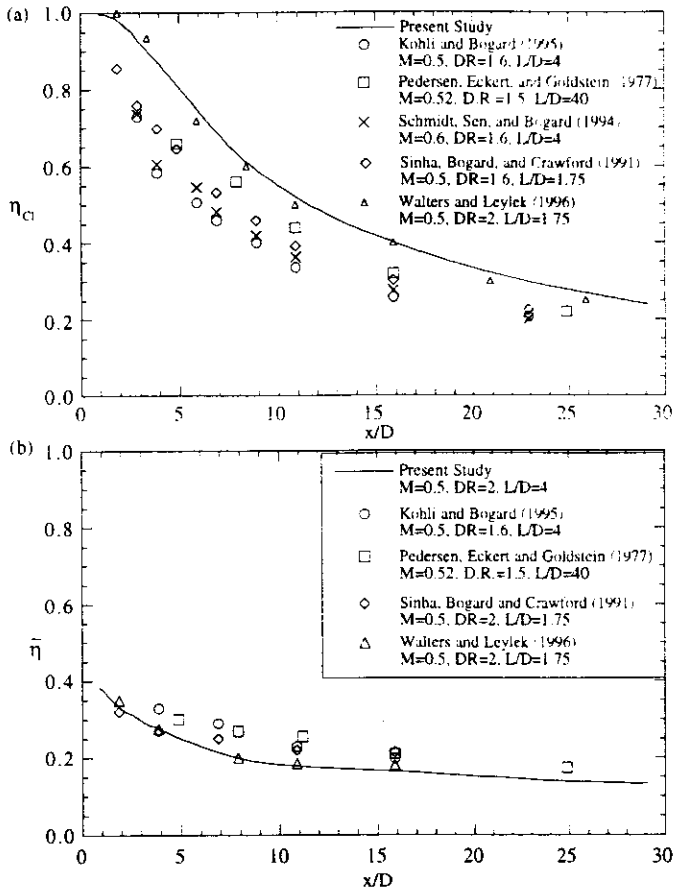

Fig. 6 (a) Centerline and (b) laterally averaged effectiveness for the round hole compared to those in the literature.

side of the hole. In the mainstream at the trailing edge of the hole exit, formation of a longitudinal vortex pair is clearly evident with the vortex cores centered at $z/D = \pm 0.5$ identified in earlier studies such as Pietrzyk, et al. (1989). On the other hand for $\phi = 90°$, flow in the supply channel causes a single swirling motion to develop inside the hole. This swirl causes flow in the cooling hole to complete one entire rotation before exiting the hole, thereby causing faster jet fluid to exit towards the -z direction, which is the same direction as the coolant supply crossflow.

The counter-rotating longitudinal vortex pair in the mainstream has been previously documented in the literature as causing a detrimental effect on the film-cooling performance by moving in 'hot' freestream fluid towards the jet centerline. Counter-rotating vortex motions have also been shown to exist inside the film-cooling hole. What has remained unclear is whether the vortex motions inside the film-cooling hole cause the longitudinal vortices or whether the freestream fluid going around the exiting jet causes the longitudinal vortices. As the results for $\phi = 90°$ show with just a single swirling jet motion, the latter is true as the longitudinal vortices are formed even though there are no counter-rotating vortices inside the cooling hole. The single swirling motion caused by the supply channel flow, however, does force the jet to come out of the hole slightly skewed resulting in the two lobes of the longitudinal vortex having different strengths.

As a benchmarking of these calculations, comparisons of the centerline and laterally averaged adiabatic effectiveness predictions were compared to those available in the literature. Figure 6 shows those com-

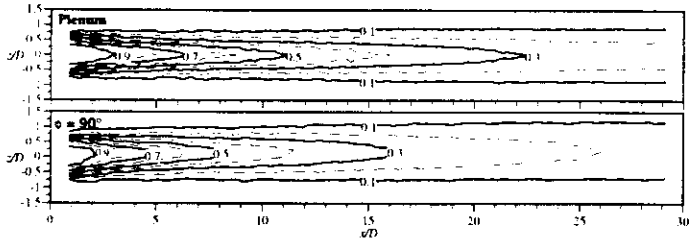

Fig. 7 Surface adiabatic effectiveness contours for the round hole with plenum condition and $\phi = 90°$.

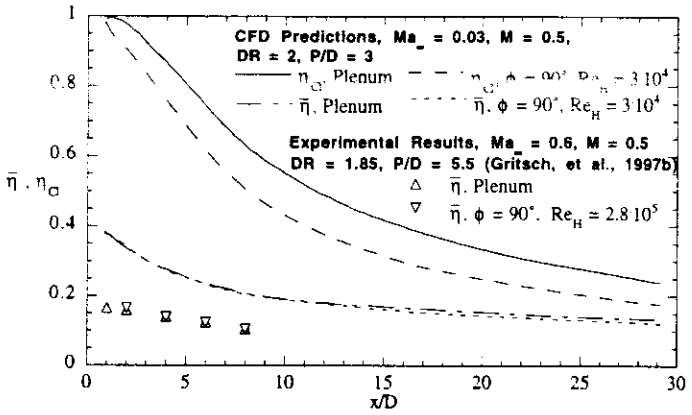

Fig. 8 Laterally averaged and centerline effectiveness for the round hole.

parisons. While the centerline effectiveness values are above those measured, these values agree well with those predicted by Walters and Leylek (1996) who used a similar CFD package. The predicted laterally averaged values also agree identically to those predicted by Walters and Leylek and show agreement with those measured.

The effect that the $\phi = 90°$ coolant supply has on the surface adiabatic effectiveness is to skew the coolant coverage as shown in Figure 7. The contours for $\phi = 90°$ show that the film-cooling jet is directed in the -z direction. Recall, the crossflow direction at the hole entrance is also in the -z direction. On comparison with the plenum case, it is evident that the maximum adiabatic effectiveness levels do not extend as far downstream for the $\phi = 90°$ case. For example, the $\eta = 0.5$ contour extends only to $x/D = 8$ for the $\phi = 90°$ case as compared with the $\eta = 0.5$ contour extending to $x/D = 11$ for the plenum case. The laterally averaged effectiveness results shown in Figure 8, however, indicate that there is not much difference between the two cases. This is because the skewed jet results in a bigger blockage to the oncoming freestream, similar to that of a compound angled cooling hole, and as a result the jet spreads more in the lateral direction. Therefore, what the jet loses in terms of the magnitude of adiabatic effectiveness, it makes up for by providing more lateral coverage. Also shown in Figure 8 is the experimental data given by Gritsch, et al. (1997b) in which there was freestream Mach number of $Ma_\infty = 0.6$. Note that their lateral averages for their single cooling hole are over a lateral distance of 5.5 hole diameters (close to two times the hole spacing simulated in these CFD studies) and, as expected, results in laterally averaged effectiveness values almost a factor of two lower than those predicted for a hole spacing of three diameters. The experimental results of Gritsch et al. also indicate that there are no differences in the laterally-averaged adiabatic effectiveness for a round hole that is subjected to either plenum supply or a strong crossflow at $\phi = 90°$.

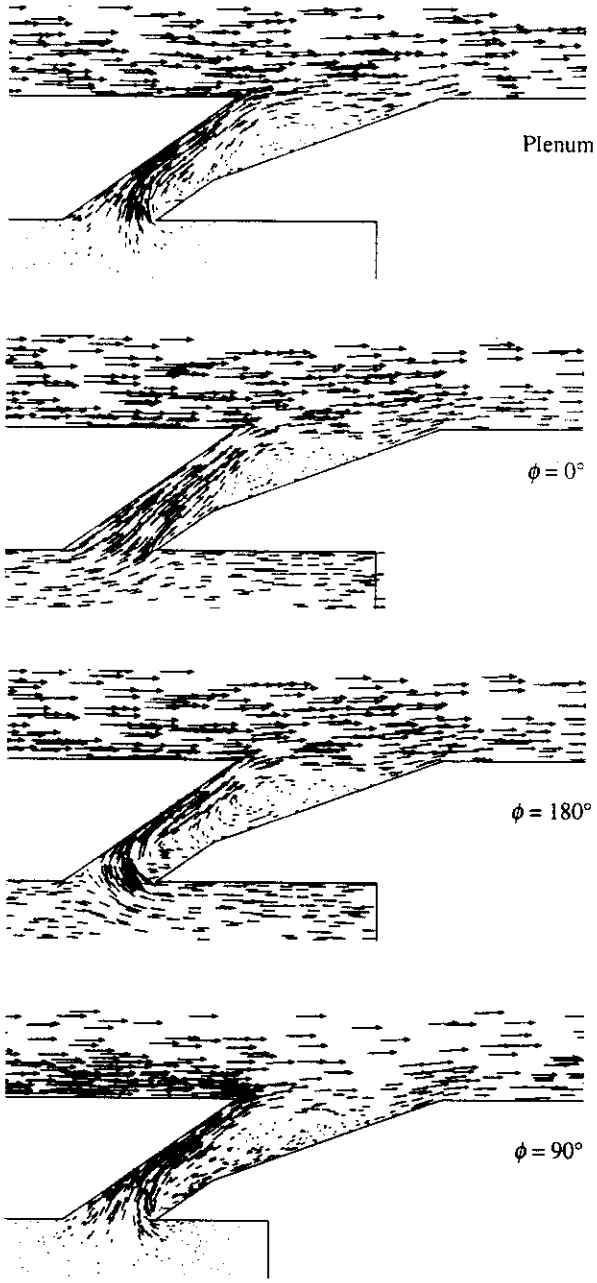

Fig. 9 Velocity vectors at the shaped hole centerline for the plenum and different flow directions in supply channel.

Shaped Hole Results

For the shaped hole calculations, the blowing and density ratios remained constant at $M = 1$ and $DR = 2$. All four entrance conditions were investigated for the shaped cooling hole. The flowfield vectors, inside the shaped cooling hole at the hole centerline are shown in Figure 9. Common to all of the entrance conditions considered for these studies is the existence of a large separation inside the expanded portion of the cooling hole. This separation region is not too surprising given the large expansion angle (15°) of the cooling hole. The separation region causes much of the coolant to flow along the windward side of the cooling hole, and in some cases, with a strong jetting action.

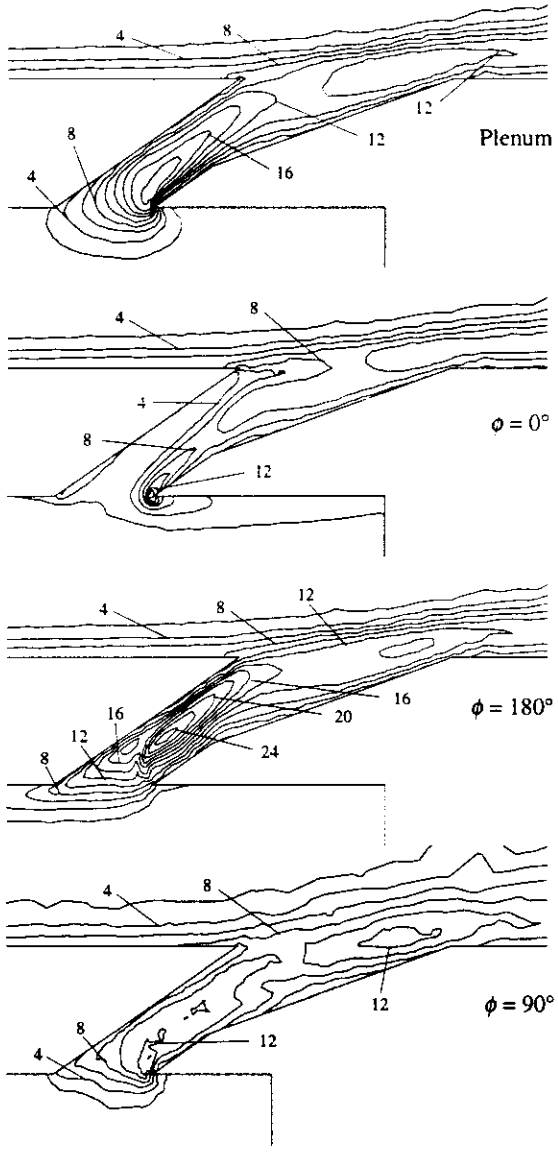

Fig. 10 Turbulence intensity contours at the shaped hole centerline for the plenum and different flow directions in supply channel.

For the plenum condition and the $\phi = 180°$ cases shown in Figure 9, another large separation region occurs at the entrance to the cooling hole that then propagates into the separation region occurring in the expansion region. At a blowing ratio of $M = 1$ and a density ratio of $DR = 2$, the velocity ratio is $VR = 0.5$. This means that the average hole velocity is one-half of the freestream velocity. The velocity magnitudes, however for the plenum and $\phi = 180°$ cases are as high as twice the average value along the windward side of the hole. The $\phi = 0°$ case indicates only small separated regions on both sides of the hole entrance and velocity magnitudes in a good portion of the hole were $V_j/U_\infty = 0.5$. The hole centerline plane for the $\phi = 90°$ case, which is not a symmetric plane, indicates low-speed fluid in the center of the hole with high-speed fluid on the windward side of the cooling hole. This low-speed region corresponds to the swirling motion that exists in the coolant hole for this case.

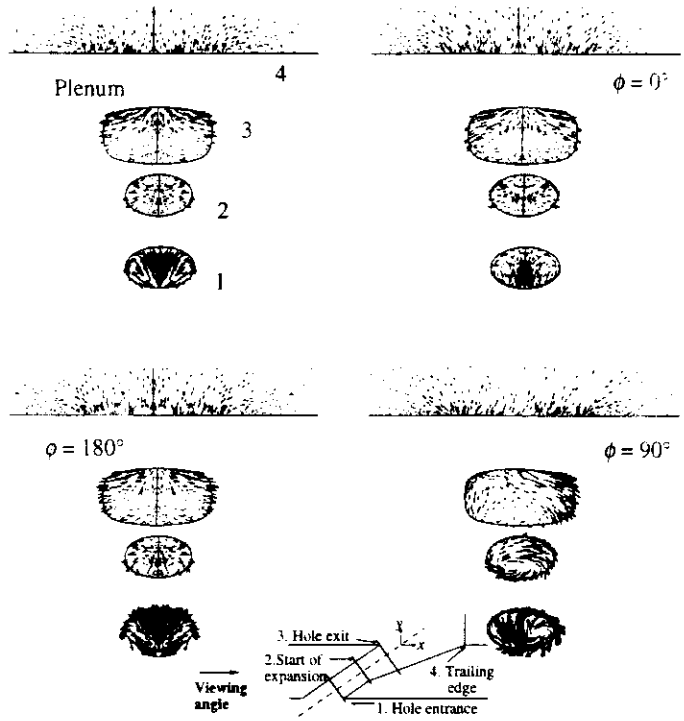

Fig. 11 Velocity vectors inside the shaped hole and at the trailing edge of the hole exit for plenum condition and different supply channel flow directions.

For both the $\phi = 0°$ and $180°$ cases, a stagnation point for the coolant can be seen. For $\phi = 0°$, the stagnation point actually occurs not at the sharp corner, but rather on the coolant channel wall slightly downstream of the leeward side of the cooling hole. For the $\phi = 180°$ case, the stagnation point occurs inside the cooling hole on the windward side.

The separation region inside the cooling hole was also hypothesized in the experimental study by Thole, et al. (1996) who measured very high turbulence levels exiting the cooling hole. Consistent with those reported turbulence levels by Thole, et al. (1996) are the high turbulence levels that were predicted by these CFD calculations as shown in Figure 10. For all of the cases predicted, the exiting turbulence levels from the holes are comparable to those measured, between $10\% \le Tu \le 14\%$. Note that the source for these high turbulence levels is the cooling hole as compared to being produced due to the mainstream/jet interaction. The peak turbulence for the plenum case, is produced as a result of the shear between the separated region and the high-speed region of the jet. In the $\phi = 0°$ case, the peak turbulence occurs at the stagnation point for the coolant fluid, but is dissipated before exiting the cooling hole resulting in the lowest exiting turbulence level in comparison to the other entrance conditions. In the $\phi = 180°$ case, which has the highest exiting turbulence level at $Tu = 14\%$ and highest turbulence level inside the cooling hole at $Tu = 24\%$, there are two distinct regions of high turbulence. These two regions include one being at the coolant stagnation point and the other being produced due to the high shear between the high and low speed fluid. For the $\phi = 90°$ case, the peak turbulence level inside the cooling hole occurs at the leeward side of the hole entrance due to the separated region.

Figure 11 shows cross-sections of the cooling hole documenting the development of the jet at various positions inside the hole and at the trailing edge of the hole, as indicated on the schematic. The vector lengths

indicate the in-plane flow directions and magnitudes. In contrast to the round hole, the shaped hole does not have any counter-rotating vortices due to the jet-mainstream interaction as indicated at the hole exit planes for all of the entrance flow conditions investigated. Similar to the round hole, however, for all of the entrance conditions except $\phi = 90^\circ$ counter-rotating vortices begin at the hole inlet and are clearly seen at the second position. The low-speed separated region at the bottom (leeward side) of the cooling holes can be seen for all of these cases, as discussed earlier, and is the largest for the $\phi = 180^\circ$ case which coincides with the strongest vortex strength.

For the $\phi = 90^\circ$ case also shown in Figure 11, there is no counter-rotating vortex but rather a single rotating vortex swirling its way through the hole. At the hole inlet, the center of the vortex is at the same side of the hole as where the coolant enters the hole. At the next two positions in the hole, the center of the vortex is at the opposite side of the hole. There is a very low-speed region occurring in the top portion of the hole on the side opposite to where the flow enters the hole. Unlike the round hole case which allowed the jet fluid to complete one rotation in the cooling hole before it exited, the shaped cooling hole only allowed the jet fluid to complete a quarter of a turn before entering the expansion. Once the jet fluid entered the hole expansion the swirling motion was no longer coherent.

Since the expansion angles of the cooling hole in both the lateral and forward directions is the same at 15°, the question arises as to whether the jet separation occurs from the bottom of the hole or from the sides of the hole. Figure 11 indicates that the flow separates from the bottom of the cooling holes as opposed to the sides. This may be, in fact, due to the vortex motions spreading the jet fluid to the lateral edges of the diffuser.

One detrimental feature of all of the shaped cooling hole cases considered in this investigation is the ingestion of 'hot' mainstream fluid into the hole. The entrainment of 'hot' mainstream into the cooling hole is a detrimental feature because of the reduction it causes to the cooling capacity of the jet. Consider the case where the supply is flowing perpendicular $\phi = 90^\circ$ to the mainstream. Figure 12 shows in-plane vectors and contours of the non-dimensional temperature, Θ, for three streamwise-vertical planes at z/D = -0.75, 0, and 0.75 also shown. At z/D = -0.75, which is on the side opposite to where the flow enters the cooling hole, the vectors clearly show the 'hot mainstream fluid' being entrained into the hole. A recirculation region occurs at the windward side of the cooling hole that entrains the hot mainstream into the hole. Although there was ingestion of 'hot mainstream fluid' into the shaped cooling hole for all cases considered, there were no recirculation regions at the hole exit on the windward side of the shaped hole identified for the plenum, $\phi = 0^\circ$ and 180° cases.

The degree of this 'hot mainstream' ingestion strongly depends on the entrance crossflow condition for the shaped cooling hole. Figure 13 shows the spatially averaged temperature, $\bar{\Theta}$, as a function of depth down into the cooling hole. Note that $y/D = 0$ is at the top of the cooling hole and y/D = -1.55 is at the start of the hole expansion. For Figure 13, the averaging for Θ was done in a streamwise-lateral plane at each vertical location where the vertical location is measured with respect to the mainstream flow. These results show that the highest degree of ingestion occurs for the $\phi = 90^\circ$ case with a value of only $\bar{\Theta} = 0.65$ at the top of the hole meaning that much of the coolant fluid was mixed with the mainstream before it had a chance to exit the hole. In addition, for the $\phi = 90^\circ$ case a $\bar{\Theta} = 1$ is not reached until one diameter inside the cooling hole. The ingestion for both the plenum and $\phi = 180^\circ$ cases, are similar and somewhat less while for the $\phi = 0^\circ$ case the least amount of ingestion occurs.

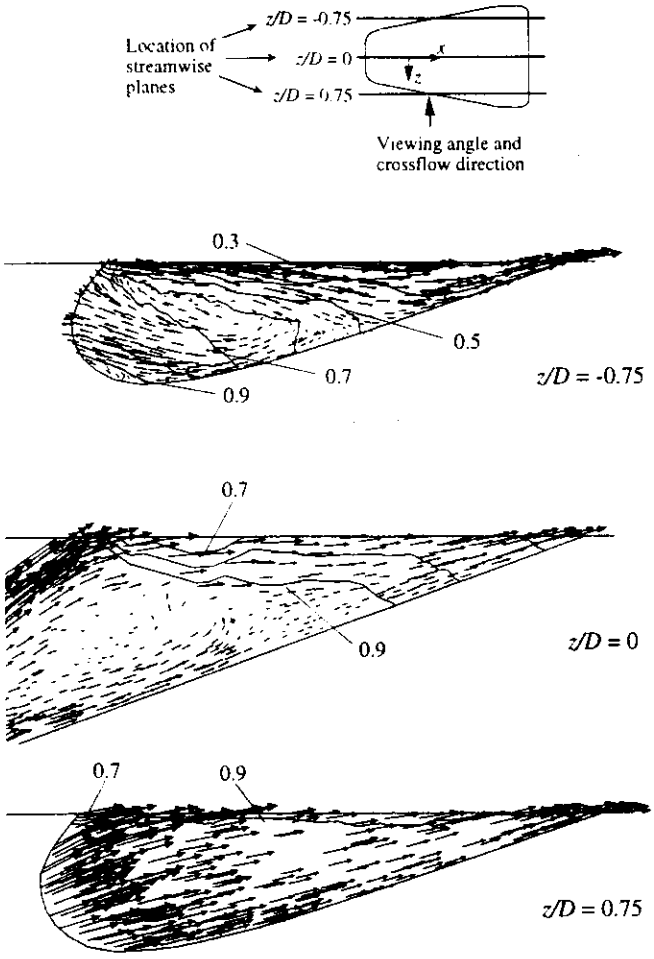

Fig. 12 Velocity vectors and normalized temperature (Θ) contours inside the shaped hole for $\phi = 90^\circ$.

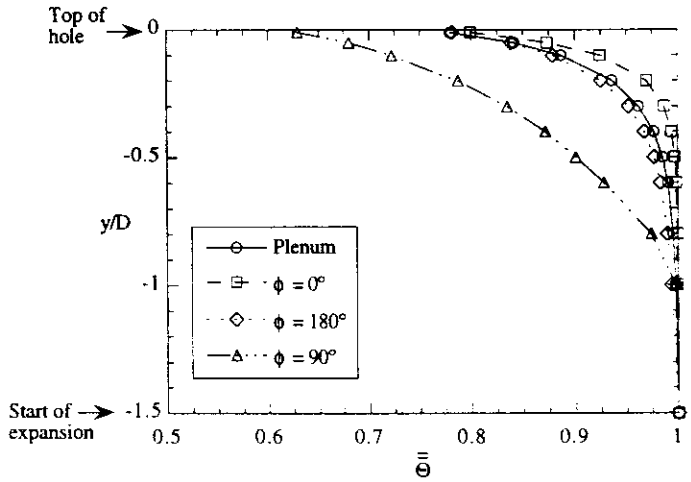

Fig. 13 Variation of normalized temperature (averaged over the x-z plane) with depth inside the shaped hole for $\phi = 90^\circ$.

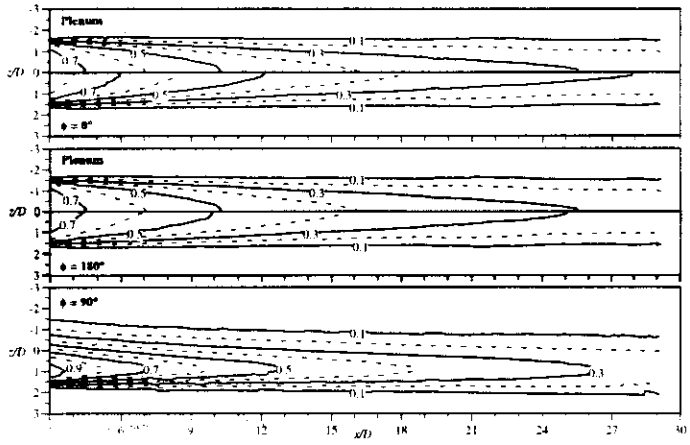

Fig. 14 Surface adiabatic effectiveness contours for the shaped hole with plenum condition and different flow directions in supply channel.

Of primary interest to the gas turbine community is the surface adiabatic effectiveness, η. The surface effectiveness contours are given in Figure 14, while the centerline, η_{cl} and laterally averaged, $\bar{\eta}$, values are given in Figures 15. Adiabatic effectiveness contours for only half the hole are given in Figure 14 for the plenum, $\phi = 0°$, and 180° cases since the flow is symmetric, whereas η contours for the full hole are given for $\phi = 90°$. Also note that results for the $\phi = 0°$ and 180° cases are placed next to the plenum case for comparison purposes.

As a benchmark, Figure 15b compares the predicted and experimentally measured (Gritsch, et al. 1997b) laterally averaged adiabatic effectiveness plot for their shaped, single cooling hole experiments. Their experiments were also done with a cooling hole having a full 15° expansion angle. There are, however, some slight geometrical differences in that their hole length was longer with an $L/D = 6$. Gritsch, et al. performed these experiments at a density ratio of $DR = 1.85$ and a blowing ratio of $M = 1$ and this can be directly compared to the CFD predictions. The agreement between experimental results and CFD predictions are very good for the plenum condition. Experimental data presented by Gritsch, et al. is also shown in Figure 15b for the cases in which the direction of the plenum is changed for the shaped film cooling hole, but at a much higher freestream Mach number of $Ma_{-} = 0.6$ and faster crossflow at the hole entrance of $Re_H = 2.8 \cdot 10^5$. The trend even at these flow conditions, however, is the same as the CFD predicted trends.

The surface contours indicate that the plenum and $\phi = 180°$ cases are very nearly the same while the results for the $\phi = 0°$ case indicates higher effectiveness values further downstream relative to the other two cases. This can also be seen in comparing the centerline and laterally-averaged adiabatic effectivenesses with higher values occurring for the $\phi = 0°$ case.

The surface contours for the $\phi = 90°$ case indicate a very skewed pattern because of the jet fluid primarily exiting towards the $+z$ direction. Recall, the round hole result for $\phi = 90°$ indicated that the jet exited toward the $-z$ direction. This difference is because the expansion in the shaped hole weakens the swirling motion and prevents it from making a complete rotation like it did in the round hole. It is not surprising that the centerline adiabatic effectiveness values are much lower than for the other three entrance conditions considered. Although the peak adiabatic effectiveness levels are higher further downstream for the $\phi = 90°$ case than for the plenum $\phi = 0°$ and 180° cases, the lateral spreading of the jet

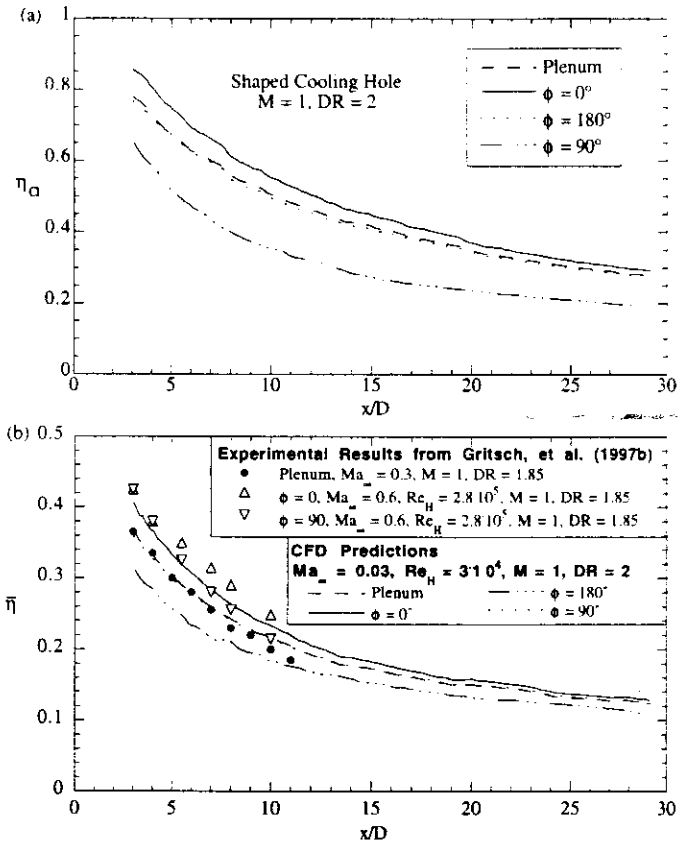

Fig. 15 (a) Centerline and (b) laterally averaged effectiveness for the shaped hole compared to that in the literature.

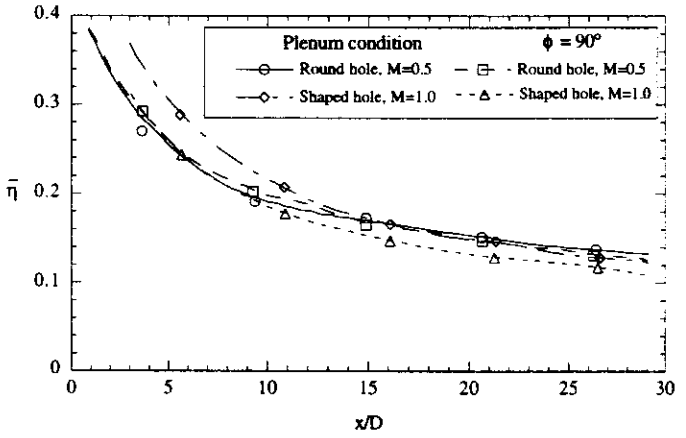

Fig. 16 Comparison of the laterally averaged effectiveness for round and shaped holes for plenum condition and ϕ= 90°.

is not very wide. In fact, the laterally-averaged effectiveness values indicate a significant decrease for the $\phi = 90°$ case especially near the hole exit. This reduced effectiveness near the hole exit is attributed to the ingestion of the mainstream fluid on one side of the hole.

Figure 16 compares the performance of the two cooling hole geometries that were considered. Although this comparison is not for the same blowing ratio through each hole, the total mass flux for the round and shaped holes would be the same per unit span, as discussed earlier. The

results indicate that a shaped cooling hole performs worse than a round cooling hole when the supply channel is flowing perpendicular to the mainstream at the exit of the hole, as is the case in most turbine applications. Future CFD and experimental studies will concentrate on evaluating the degree of ingestion that causes the reduction in effectiveness from a shaped cooling hole, at higher blowing ratios.

CONCLUSIONS

These CFD predictions indicate that at the near-optimal blowing ratio ($M = 0.5$) for a round cooling hole having an $L/D = 4$, the laterally-averaged values of surface adiabatic effectiveness are the same whether the coolant hole entrance is supplied by a plenum or by a channel that is turned perpendicular to the mainstream flow direction. The results also indicate, however, that counter-rotating vortices occur inside the hole when the coolant is supplied by a plenum, as opposed to a single swirl motion that completes one revolution inside the hole when the coolant is supplied with a perpendicular crossflow. No matter which flow pattern occurs inside the hole, the longitudinal counter-rotating vortices in the mainstream, due to the mainstream fluid going around the jet, still occur.

These CFD results indicate that the flowfield inside a fully expanded cooling hole at 15° is quite complex. For all of the entrance crossflow conditions considered, a large separation occurs in the expanded portion of the cooling hole. Considering that many turbine blade designs rely on convective cooling from the flow going through the hole, this separation is not desirable.

The surface adiabatic effectiveness values for the plenum and the counter-flowing supply channel are quite similar while a slight improvement is achieved with the co-flowing supply channel. Unlike the round hole, the effectiveness deteriorates when the hole entrance is subjected to a crossflow that is perpendicular. This deterioration is caused by the significant amount of ingestion of 'hot' mainstream fluid into the cooling hole. The skewed jet velocity profile exiting the cooling hole results in a recirculation region on the windward side of the hole exit which was identified as the mechanism causing mainstream ingestion into the hole.

These results indicate that a turbine designer, given an allowable coolant mass flux as simulated in these predictions and knowing that the crossflow at the hole entrance is perpendicular to the mainstream, should use a round cooling hole. A round hole should be strongly considered because its effectiveness performance is comparable to the shaped hole; because it's less sensitive to the coolant supply condition at the hole entrance; because there is potentially higher convective heat transfer within the round holes as opposed to the separated flow in the shaped holes; and because of the lower manufacturing costs.

ACKNOWLEGEMENT

The authors would like to thank the National Science Foundation's CAREER program with Drs. Deborah Kaminski and Timothy Tong as program directors.

REFERENCES

Berhe, M. K. and Patankar, V. (1996) "A Numerical Study of Discrete-Hole Film Cooling," ASME Paper No. 96-WA/HT-8.

FLUENT User's Guide (1996) Fluent Incorporated, Lebanon, New Hampshire.

Garg, V. K. and Gaugler, R. E. (1995) "Effect of Velocity and Temperature Distribution at the Hole Exit on Film Cooling of Turbine Blades," ASME Paper No. 95-GT-2.

Goldstein, R. J., Eckert, E. R. G., and Burggraf, F. (1974) "Effects of Hole Geometry and Density on Three-Dimensional Film Cooling," *International Journal of Heat and Mass Transfer*, vol. 17, pp. 595-607.

Gritsch, M., Schulz, A., and Wittig, S. (1997a) "Discharge Coefficient Measurements of Film-Cooling Holes with Expanded Exits," to be presented at the International Gas Turbine and Aeroengine Congress and Exposition, Orlando, Florida.

Gritsch, M., Schulz, A., and Wittig, S. (1997b) "Adiabatic Wall Effectiveness Measurements of Film-Cooling Holes with Expanded Exits," to be presented at the International Gas Turbine and Aeroengine Congress and Exposition, Orlando, Florida.

Han, J. C. (1984) "Heat Transfer and Friction in Channels with Two Opposite Rib-Roughened Walls," ASME *Journal of Heat Transfer*, Vol. 106, pp. 774-781.

Hay, N., Lampard, D., and Benmansour, S. (1983) "Effect of Crossflows on the Discharge Coefficient of Film Cooling Holes," *ASME Journal of Engineering for Power*, Vol. 105, pp. 243-248.

Kim, S. and Choudhury, D. (1995) "A Near-Wall Treatment Using Wall Functions Sensitized to Pressure Gradient," ASME Fluids Engineering Div. Summer Conference, Hilton Head, South Carolina.

Launder, B. E. and Spalding, D. B. (1974) "The Numerical Computation of Turbulent Flows," *Computer Methods in Applied Mechanics and Engineering*, Vol. 3, pp. 269-289.

Leylek, J. H. and Zerkle, R. D. (1994) "Discrete-Jet Film Cooling: A Comparison of Computational Results with Experiments," *ASME Journal of Turbomachinery*, Vol. 116, pp. 358-368.

Pedersen, D. R., Eckert, E. R. G., and Goldstein, R. J. (1977) "Film Cooling with Large Density Differences Between the Mainstream and the Secondary Fluid Measured by the Heat-Mass Transfer Analogy," *ASME Journal of Heat Transfer*, vol. 99, pp. 620-627.

Pietrzyk, J. R., Bogard, D. G., and Crawford, M. E. (1989) "Hydrodynamic Measurements of Jets in Crossflow for Gas Turbine Film Cooling Application," *ASME Journal of Turbomachinery*, Vol. 111, pp. 1139-145.

Schmidt, D. L., Sen, B., and Bogard, D. G. (1996) "Film Cooling with Compound Angle Holes: Heat Transfer," *ASME Journal of Turbomachinery*, Vol. 118, pp. 800-806.

Sinha, A. K., Bogard, D. G., Crawford, M. E. (1991) "Film Cooling Effectiveness Downstream of a Single Row of Holes with Variable Density Ratio," *ASME Journal of Turbomachinery*, Vol. 113, pp. 442-449.

Thole, K. A., Gritsch, M., Schulz, A., and Wittig, S. (1996) "Flowfield Measurements for Film Cooling Holes with Expanded Exits," ASME Paper No. 96-GT-174.

Thole, K. A., Gritsch, M., Schulz, A., and Wittig, S. (1997) "Effect of a Crossflow at the Entrance to a Film-Cooling Hole," to appear in the *ASME Journal of Fluid Engineering*.

Walters, D. K. and Leylek, J. H. (1995) "A Systematic Computational Methodology Applied to a Three-Dimensional Film-Cooling Flowfield," ASME Paper No. 96-GT-351.

Wittig, S., Schulz, A., Gritsch, M., and Thole, K. A. (1996) "Transonic Film Cooling Investigations: Effects of Hole Shapes and Orientations," ASME Paper No. 96-GT-222.